Strong Amplification of Coherent Acoustic Phonons by Intraminiband Currents in a Semiconductor Superlattice

Keisuke Shinokita,[1] Klaus Reimann,[1] Michael Woerner,[1] Thomas Elsaesser,[1] Rudolf Hey,[2] and Christos Flytzanis[3]
[1]Max-Born-Institut für Nichtlineare Optik und Kurzzeitspektroskopie, 12489 Berlin, Germany
[2]Paul-Drude-Institut für Festkörperelektronik, 10117 Berlin, Germany
[3]Laboratoire Pierre Aigrain, École Normale Supérieure, 75231 Paris, France
(Received 13 November 2015; published 18 February 2016)

Sound amplification in an electrically biased superlattice (SL) is studied in optical experiments with 100 fs time resolution. Coherent SL phonons with frequencies of 40, 375, and 410 GHz give rise to oscillatory reflectivity changes. With currents from 0.5 to 1.3 A, the Fourier amplitude of the 410 GHz phonon increases by more than a factor of 2 over a 200 ps period. This amplification is due to stimulated Čerenkov phonon emission by electrons undergoing intraminiband transport. The gain coefficient of 8×10^3 cm^{-1} is reproduced by theoretical calculations and holds potential for novel sub-THz phonon emitters.

DOI: 10.1103/PhysRevLett.116.075504

The interaction of acoustic phonons with electrons plays a fundamental role for the transient electronic, optical, and transport properties of solids. Extensive work on incoherent phonon generation by hot-carrier relaxation [1,2] has been complemented recently by the optical generation of coherent acoustic phonons in bulk and low-dimensional semiconductors [3–6]. Propagating and standing acoustic waves have been mapped in space and time by time-resolved optical and x-ray techniques [7–9]. Of particular interest are schemes for amplifying acoustic phonons by interaction with moving electrons. Such sound amplification is based on the stimulated emission of acoustic phonons, bosonic elementary excitations, upon transitions of the carriers between different electronic states. So far, experimental studies of acoustic phonon amplification have remained scarce, in particular in the gigahertz frequency range.

One concept of acoustic phonon amplification has exploited stimulated phonon emission by a vertical tunneling or hopping current of electrons in a semiconductor superlattice (SL). In this way, propagating incoherent [10] and coherent phonons [11] at sub-THz frequencies have been amplified by up to 45 percent. Stimulated phonon emission occurs between quantized electronic states in a Wannier-Stark ladder of the biased SL. The amplification displays a resonance at a Stark splitting corresponding to the phonon energy; i.e., the frequency of amplified phonons is set by the electrical bias. The electric tunneling current in the SL is limited to typically 10^{-3} A, resulting in a limited phonon amplification factor.

The so-called Čerenkov emission represents a basically different approach, in which an intraband electron current interacts with copropagating acoustic phonons [12–17]. In bulk semiconductors, the acoustic wave sets up a spatial modulation of the electron density and exchanges energy with the electrons via the deformation potential and piezoelectric interactions. Under bias, the fraction of electrons with a kinetic energy higher than the phonon energy is enhanced, resulting in an enhanced stimulated emission of acoustic phonons and, thus, a net amplification of the acoustic wave. While this scenario has been analyzed extensively by theory [14–16], the few experimental studies have remained limited to phonon frequencies below 100 MHz [13,17].

In this Letter, we demonstrate a novel concept of acoustic phonon amplification at sub-THz frequencies. Impulsive phonon excitation by a femtosecond optical pulse generates coherent SL phonons propagating forward and backward along the SL stack axis, i.e., a standing acoustic wave. Interaction of the copropagating wave with an electrically driven electron current allows for phonon amplification via the Čerenkov mechanism, connected with electron transitions between states within an electronic miniband. The intraminiband character of the electron transport allows for much higher currents than electron tunneling and, thus, a much stronger phonon amplification by more than 200%.

The GaAs/$Al_{0.3}Ga_{0.7}As$ SL [Fig. 1(a)] studied at ambient temperature (300 K) was grown by molecular beam epitaxy on a 360 μm-thick (001)-oriented GaAs substrate. It contains 70 SL periods, each consisting of a 9.7 nm thick GaAs well and a 1.7 nm thick $Al_{0.3}Ga_{0.7}As$ barrier layer. The GaAs layers are n doped with a concentration of 5.2×10^{15} cm^{-3}. The thin $Al_{0.3}Ga_{0.7}As$ barrier layers allow for electronic coupling of neighboring GaAs layers and the formation of minibands. The lowest conduction miniband has a width of 20 meV.

The SL is embedded in highly n-doped ($n = 5 \times 10^{18}$ cm^{-3}) 55 nm- and 100 nm-thick GaAs layers. On top of the structure, there is a ringlike silver contact surrounding a surface area of 0.3 mm^2. The bottom surface of the substrate is covered by a metal layer system serving as the electric contact. Square-wave current pulses are applied in forward bias from the top to the substrate side

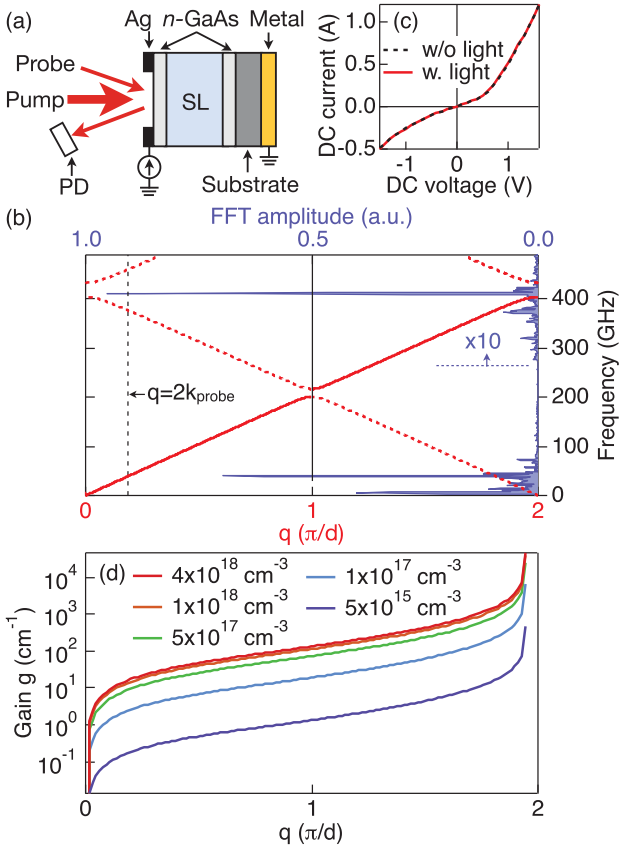

FIG. 1. (a) Schematic of the superlattice (SL) structure and the pump-probe reflection geometry. The bottom metal contact consists of a Au/Ge/Ni alloy. (b) Red lines: Calculated dispersion of longitudinal SL phonons in the first mini-Brillouin zone. The phonon frequency is plotted as a function of the phonon q vector. The black line marks the q vector of phonons generated via a Raman process. Blue line: Fourier spectrum of the coherent reflectivity oscillations measured with the unbiased sample [upper abscissa scale, cf. the black trace in Fig. 2(b)]. The spectrum displays major frequency components at 40, 375, and 410 GHz. (c) Current-voltage characteristics of the sample with and without photoexcitation. (d) Phonon gain coefficient $g = \Gamma_q / v_{\text{sound}}$ calculated for deformation potential coupling as a function of the phonon q vector for different carrier densities.

along the (001) direction with a repetition rate of 20 Hz and a duty cycle of 20%.

The SL period of $d = 9.7 + 1.7 = 11.4$ nm leads to the formation of a mini-Brillouin zone with a width of $2\pi/d$ and to a confinement of acoustic phonons by the SL, resulting in a back-folded phonon dispersion [18]. The calculated longitudinal SL phonon dispersion is shown in Fig. 1(b). Its main features are higher SL phonon branches originating from the acoustic phonons of the bulk material and small energy gaps at the zone boundaries due to the different mass densities and speeds of sound of GaAs and $Al_{0.3}Ga_{0.7}As$.

In the optical pump-probe experiments, a pump pulse excites the SL sample through the upper surface. A delayed probe pulse measures the spectrally integrated change of reflectivity as a function of pump-probe delay. Pump and probe pulses of 100 fs duration and a center wavelength of 845 nm (photon energy of 1.467 eV) are derived from the output of a mode-locked Ti:sapphire oscillator with an 80 MHz repetition rate. The spectral bandwidth of the pulses is 20 nm (35 meV). The average pump power of 120 mW is focused to a spot diameter of 40 μm, resulting in an excitation density of $N_{\text{ex}} \approx 10^{18}$ electron-hole pairs per cm^3. The average probe power is 3 mW. The reflected light is detected with a photodiode. Its electrical signal is fed into a lock-in amplifier selecting the photocurrent component occurring at a 20 Hz frequency.

A first set of time-resolved reflectivity data was measured with the unbiased sample. The pump-probe traces show a steplike decrease of reflectivity [Fig. 2(a)]. The sign of the reflectivity change depends on the spectral position of the pulses relative to the (shifted) band gap of the excited sample [19]. In our case, the relative spectral position is different from the experiments of Ref. [11] where an increase of reflectivity was seen. The steplike reflectivity change of Fig. 2(a) is superimposed by pronounced oscillations, shown in Fig. 2(b) (black line) after subtraction of the steplike signal. A Fourier analysis of the oscillatory transient gives the spectrum in Fig. 1(b). The frequency components at 40 and 375 GHz are due to SL phonons Raman excited within the spectral bandwidth of the pump pulses at the q-vector value marked in Fig. 1(b) (dashed vertical line). In contrast, coherent SL phonons at 410 GHz are generated by a displacive mechanism, as discussed below.

An electrical bias on the sample generates an intraminiband current of electrons. The current-voltage characteristics shown in Fig. 1(c) are identical with and without illumination of the SL sample by the femtosecond pulse train. Under forward bias with 1 to 2 V, currents on the order of 1 A occur, roughly 3 orders of magnitude higher than the tunneling currents in Ref. [11]. The transient rise of sample temperature is less than 10 K, as measured with a calibrated thermocamera.

The oscillatory component of a reflectivity transient measured for a current of $I = 1$ A is shown in Fig. 2(b) (red line). For all delay times, bias increases the oscillation amplitude, as evident from the difference of the two time traces plotted in Fig. 2(c). Fourier spectra of the time traces of Fig. 2(b) with and without current are presented in Fig. 2(g) and display frequency components originating from all coherently excited SL phonons. For all components, the Fourier amplitudes are enhanced under bias (red line, $I = 1$ A) compared to the unbiased sample ($I = 0$ A, black line). The linewidths with and without current are identical, being determined by the finite time window of our measurements. For a more detailed analysis, we bandpass filtered the differential trace of Fig. 2(c) in different frequency windows. Figure 2(d) shows the results

around 40 GHz, and Figs. 2(e) and 2(f) around 410 GHz. It is important to note that the amplitude of the 40 GHz component is independent of the pump-probe delay, while the 410 GHz amplitude increases strongly on a 200 ps time scale. The 410 GHz component has the same phase with and without current over the whole delay range [300 ps, Fig. 2(f)], ruling out current-induced changes of phonon frequencies.

The enhancement of the 410 GHz Fourier amplitude depends on the electric current through the SL (Fig. 3). Figures 3(a) and 3(b) show the oscillatory time traces and the related Fourier spectra. The results provide clear evidence for a monotonic increase of phonon amplitude with current. This behavior is shown in Fig. 3(c), displaying the Fourier amplitudes of the 410 GHz SL phonon as a function of current. The data exhibit a threshold around 0.5 A and a roughly linear increase at higher currents.

We now discuss our key result, the increase of the Fourier amplitude of the 410 GHz SL phonon oscillations with current and time. In our experiments, the photon energies of the pump and probe pulses are in the range of the interband absorption from the highest valence to the lowest conduction miniband. The penetration depth of the pump pulses, which excite coherent SL phonons, is

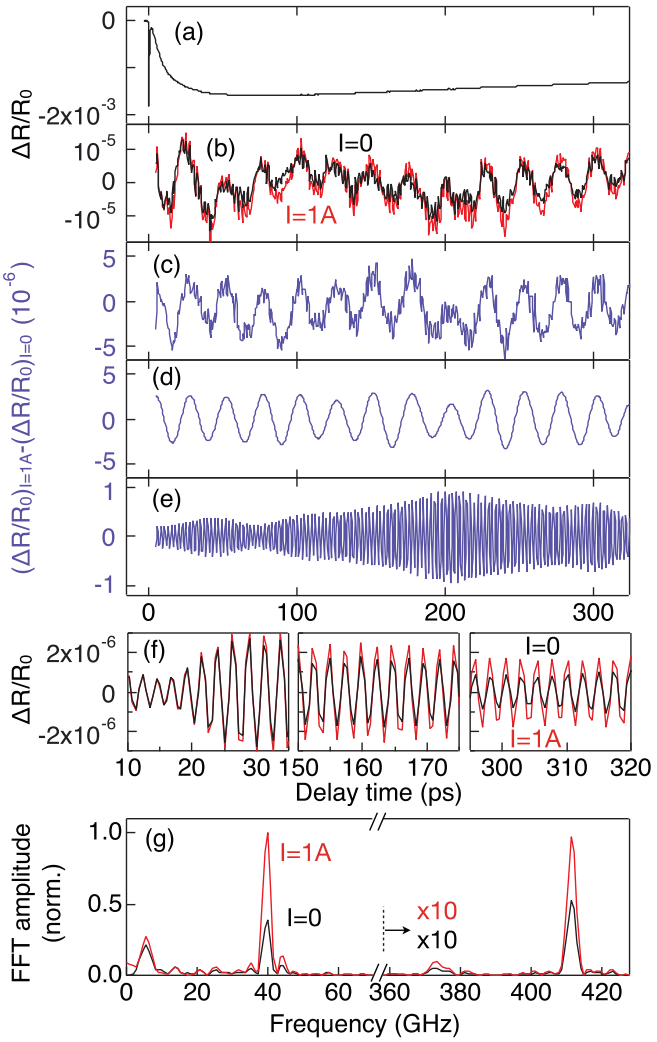

FIG. 2. (a) Time-resolved reflectivity change of the SL sample measured without electrical bias. The change of reflectivity $\Delta R/R_0 = (R - R_0)/R_0$ is plotted as a function of pump-probe delay (R and R_0 are the reflectivity with and without excitation). (b) Oscillatory component of the time-resolved reflectivity change with (current $I = 1$ A, red line) and without electrical bias ($I = 0$ A, black line). (c) Differential reflectivity change $\Delta R/R_0(I = 1\text{A}) - \Delta R/R_0(I = 0\text{A})$, corresponding to the difference of the two transients in Fig. 2(b). Differential reflectivity change in two frequency ranges, (d) between 30 and 50 GHz and (e) between 400 and 420 GHz. The increase in amplitude with delay time in (e) is due to acoustic phonon amplification. (f) Differential reflectivity with (red) and without (black) current in the frequency range between 400 and 420 GHz. (g) Fourier spectra of the oscillatory reflectivity changes measured with and without current [red and black line, cf. Fig. 2(b)].

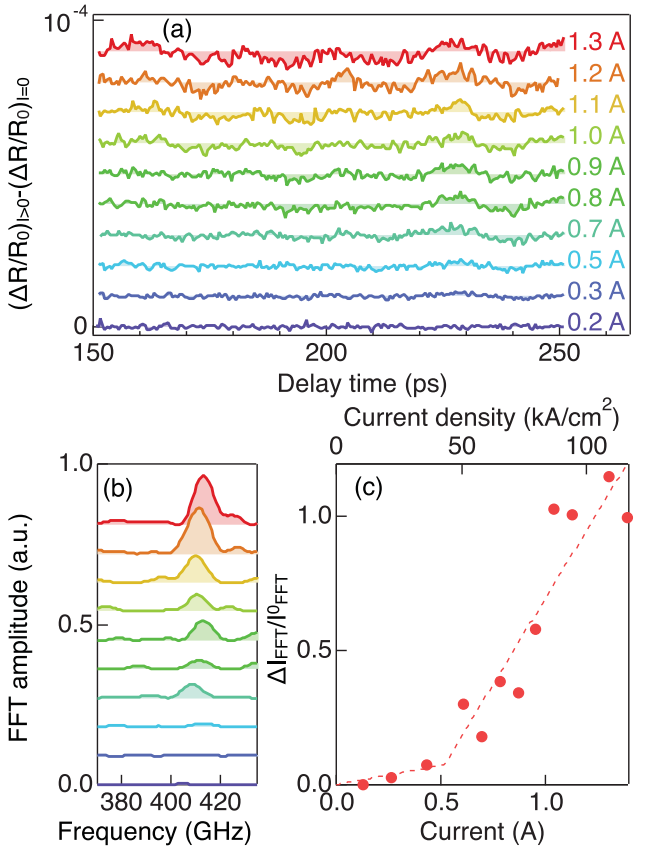

FIG. 3. (a) Oscillatory component of the time-resolved reflectivity change for different currents through the SL structure. (b) Fourier spectra of the transients in part (a). (c) Change of the Fourier amplitude of the 410 GHz oscillations (dots) as a function of current, normalized to the value without current. The dotted line represents a bilinear fit, yielding a threshold value of $I \approx 0.5$ A for phonon amplification. The upper scale gives the current density assuming that the current only flows through the optically pumped volume.

comparable to the thickness of the SL structure, so that coherent phonons are generated in the whole SL rather than at the surface of the sample. The phonon oscillations are detected via reflectivity changes of the probe pulses. Reference measurements with a spectrally dispersed detection of the probe reveal a spectrum of the reflectivity change unaffected by the electrical bias. Thus, a bias-induced change of the SL's dielectric function can be ruled out as an explanation for the enhanced Fourier amplitudes of the coherent phonons.

The coherent SL phonon at 410 GHz is excited via a displacive mechanism [9], originating from the spatially periodic absorption of pump light in the GaAs layers of the SL. Photoexcited carriers in the GaAs layers generate via the deformation potential interaction a spatially periodic stress pattern that drives the SL phonon at 410 GHz. This mechanism results in coherent phonons spatially delocalized over the SL. They correspond to standing SL phonon waves, i.e., a coherent superposition of forward and backward traveling acoustic waves with dephasing times on the order of 100 ps [cf. the long-lasting oscillations in Fig. 2(e)].

Under bias, the intraminiband current of electrons interacts with the coherent phonon excitation mainly via the acoustic deformation potential. Piezoelectric coupling [20] is weak because of the lattice symmetry and screening at the high electron densities present. Electrons with kinetic energies higher than the SL phonon energy enhance the coherent amplitude by the stimulated intraband emission of acoustic phonons, exploiting the population inversion between electronic states in the same miniband. This so-called Čerenkov mechanism acts mainly on the acoustic wave traveling in the forward direction, i.e., in the same direction as the electrons. In other words, the electric bias shifts the Fermi distribution of electrons to larger k vectors, introducing an asymmetric carrier distribution in k space and enabling phonon amplification.

The time evolution of the 410 GHz Fourier amplitude as shown in Fig. 2(e) and the threshold behavior shown in Fig. 3(c) provide strong support for this picture. The amplitude grows over a period of $t \approx 200$ ps. In this time interval, the coherent acoustic wave travels a distance $l = v_{\text{sound}} t \approx 0.9\ \mu$m, assuming an average velocity of sound $v_{\text{sound}} = 4700$ m/s. This value of l is very close to the overall SL thickness of 0.8 μm, suggesting an amplification process over all periods of the SL. Using $l = 0.9\ \mu$m and the measured amplification factor of about 2 [Fig. 3(a)], one estimates an effective acoustic gain coefficient of 8×10^3 cm^{-1}, much higher than what has been observed with SL tunneling currents. To estimate the threshold current I_T for amplification, we assume that stimulated emission sets in when the electron drift velocity reaches the sound velocity. The current is given by $I_T = nev_{\text{sound}}S$ (e is the elementary charge). With the density of photoexcited carriers $N_{\text{ex}} = 10^{18}$ cm^{-3} and the optical spot size $S = 1.2 \times 10^{-5}$ cm^2, one estimates a value of $I_T \approx 0.9$ A, close to the measured value of approximately 0.5 A.

For a theoretical estimate of the phonon gain coefficient, we use the formalism of Refs. [16] and [21]. According to Eq. (16) of Ref. [21] for the phonon transition rate

$$\Gamma_{\mathbf{q}} = \frac{2\pi}{\hbar}|C_{\mathbf{q}}|^2 \frac{V}{(2\pi)^3}\int d\mathbf{k}(f_{\mathbf{k}} - f_{\mathbf{k}-\mathbf{q}}) \times \delta[\varepsilon_{\mathbf{k}} - \varepsilon_{\mathbf{k}-\mathbf{q}} - (\hbar\omega_{\mathbf{q}} - \hbar\mathbf{q}\mathbf{v}_D)] \quad (1)$$

we calculated the phonon gain coefficient $g = \Gamma_{\mathbf{q}}/v_{\text{sound}}$ due to the acoustic deformation potential interaction $|C_{\mathbf{q}}^{\text{dp}}|^2 = \Xi^2\hbar q/(V2\rho v_{\text{sound}})$ ($f_{\mathbf{k}}$ is the Fermi distribution at $T = 300$ K). The coupling parameters were taken from Tables 1.8, 3.4, and 3.6 of Ref. [20]. In Fig. 1(d), results are plotted for a drift velocity of $v_D = 2v_{\text{sound}}$ and different electron densities. The calculations show that the gain coefficient g increases strongly with q, reflecting the q dependence of the acoustic deformation potential. The gain coefficient increases roughly linearly with electron density up to $N = 10^{17}$ cm^{-3} and then starts to saturate. For the density $N_{\text{ex}} = 10^{18}$ cm^{-3} of carriers photoexcited in our experiments, we find a value of $g \approx 10^4$ cm^{-1} for the SL phonon at the outer edge of the mini-Brillouin zone, in good agreement with the experimental value of 8×10^3 cm^{-1}.

A comment should be made on the bias-induced amplitude enhancement of the Raman-excited coherent phonons at 40 and 375 GHz [cf. Fig. 2(g)]. As shown in panel (d) for the 40 GHz phonon, this enhancement is independent of the pump-probe delay and, thus, cannot be caused by phonon amplification. In view of the very small changes of sample temperature, thermal effects are excluded as well. Instead, it originates from a current-induced increase of the Raman scattering amplitudes. More specifically, before the arrival of the pump pulse the drift current of the electrons present by doping tends to enhance the quasistationary nonequilibrium phonon population to a value of [see Eq. (10) of Ref. [21]]

$$N_{\mathbf{q}}^0(\mathbf{v}_D, T) = \left[\exp\left(\frac{\hbar\omega_{\mathbf{q}} - \hbar\mathbf{q}\mathbf{v}_D}{k_B T}\right) - 1\right]^{-1}, \quad (2)$$

in competition with anharmonic phonon-phonon interactions tending to establish a Bose distribution of phonons at lattice temperature T, i.e., $N_{\mathbf{q}}^0(\mathbf{v}_D = 0, T)$. The bias-induced enhanced phonon population increases the signal amplitude of spontaneous Raman scattering [see Eq. (29) of Ref. [22]] and of the impulsive coherent Raman excitation and probing as done in our experiments for the phonons at 40 and 375 GHz.

In conclusion, we have demonstrated the strong amplification of coherent acoustic phonons in a semiconductor superlattice at room temperature. Amplification is based on

the stimulated emission of acoustic phonons by electrically driven electrons undergoing intraminiband transport. This mechanism allows for a strong amplification of displacively excited superlattice phonons. In our present superlattice these phonons have a frequency of 410 GHz. By changing the width of the superlattice layers, the amplified phonon frequency can be chosen in a wide range. Our amplification concept holds potential for intense sources of coherent acoustic phonons in the sub-THz frequency range and may become a key ingredient of devices based on sound amplification by stimulated emission of radiation (SASER) [23,24]. With such sources of sub-THz coherent phonons it will be possible to study phonon propagation and dephasing with much higher sensitivity and precision than presently possible. Phonons with sub-THz frequencies have wavelengths in the nanometer range, allowing for investigations with very high spatial resolution, e.g., in microelectronic devices or in microbiology.

We thank Dr. Klaus Biermann for help with the sample. K. S. appreciates the support of the JSPS Postdoctoral Fellowship for Research Abroad (27-830).

[1] Nonequilibrium Phonon Dynamics, edited by W. E. Bron (Plenum Press, New York, 1984).
[2] B. K. Ridley, Hot phonons in high-field transport, Semicond. Sci. Technol. **4**, 1142 (1989).
[3] M. M. Robinson, Y.-X. Yan, E. B. Gamble, Jr., L. R. Williams, J. S. Meth, and K. A. Nelson, Picosecond impulsive stimulated Brillouin scattering: Optical excitation of coherent transverse acoustic waves and application to time-domain investigations of structural phase transitions, Chem. Phys. Lett. **112**, 491 (1984).
[4] A. Yamamoto, T. Mishina, Y. Masumoto, and M. Nakayama, Coherent Oscillation of Zone-Folded Phonon Modes in Gaas-Alas Superlattices, Phys. Rev. Lett. **73**, 740 (1994).
[5] A. Bartels, T. Dekorsy, H. Kurz, and K. Köhler, Coherent Zone-Folded Longitudinal Acoustic Phonons in Semiconductor Superlattices: Excitation and Detection, Phys. Rev. Lett. **82**, 1044 (1999).
[6] K. Mizoguchi, M. Hase, S. Nakashima, and M. Nakayama, Observation of coherent folded acoustic phonons propagating in a GaAs/AlAs superlattice by two-color pump-probe spectroscopy, Phys. Rev. B **60**, 8262 (1999).
[7] C. Thomsen, H. T. Grahn, H. J. Maris, and J. Tauc, Surface generation and detection of phonons by picosecond light pulses, Phys. Rev. B **34**, 4129 (1986).
[8] A. M. Lindenberg, I. Kang, S. L. Johnson, T. Missalla, P. A. Heimann, Z. Chang, J. Larsson, P. H. Bucksbaum, H. C. Kapteyn, H. A. Padmore, R. W. Lee, J. S. Wark, and R. W. Falcone, Time-Resolved X-Ray Diffraction from Coherent Phonons During a Laser-Induced Phase Transition, Phys. Rev. Lett. **84**, 111 (2000).
[9] M. Bargheer, N. Zhavoronkov, Y. Gritsai, J. C. Woo, D. S. Kim, M. Woerner, and T. Elsaesser, Coherent atomic motions in a nanostructure studied by femtosecond x-ray diffraction, Science **306**, 1771 (2004).
[10] A. J. Kent, R. N. Kini, N. M. Stanton, M. Henini, B. A. Glavin, V. A. Kochelap, and T. L. Linnik, Acoustic Phonon Emission from a Weakly Coupled Superlattice under Vertical Electron Transport: Observation of Phonon Resonance, Phys. Rev. Lett. **96**, 215504 (2006).
[11] R. P. Beardsley, A. V. Akimov, M. Henini, and A. J. Kent, Coherent Terahertz Sound Amplification and Spectral Line Narrowing in a Stark Ladder Superlattice, Phys. Rev. Lett. **104**, 085501 (2010).
[12] R. H. Parmenter, The acousto-electric effect, Phys. Rev. **89**, 990 (1953).
[13] G. Weinreich and H. G. White, Observation of the acousto-electric effect, Phys. Rev. **106**, 1104 (1957).
[14] H. N. Spector, Amplification of acoustic waves through interaction with conduction electrons, Phys. Rev. **127**, 1084 (1962).
[15] For a review, see N. I. Meyer and M. H. Jørgensen, in *Festkörperprobleme X*, edited by O. Madelung (Vieweg, Braunschweig, 1970). pp. 21–124.
[16] S. M. Komirenko, K. W. Kim, A. A. Demidenko, V. A. Kochelap, and M. A. Stroscio, Generation and amplification of sub-THz coherent acoustic phonons under the drift of two-dimensional electrons, Phys. Rev. B **62**, 7459 (2000).
[17] A. R. Hutson, J. H. McFee, and D. L. White, Ultrasonic Amplification in CdS, Phys. Rev. Lett. **7**, 237 (1961).
[18] C. Colvard, T. A. Gant, M. V. Klein, R. Merlin, R. Fischer, H. Morkoc, and A. C. Gossard, Folded acoustic and quantized optic phonons in (GaAl)As superlattices, Phys. Rev. B **31**, 2080 (1985).
[19] S. H. Park, J. F. Morhange, A. D. Jeffery, R. A. Morgan, A. Chavez-Pirson, H. M. Gibbs, S. W. Koch, N. Peyghambarian, M. Derstine, A. C. Gossard, J. H. English, and W. Weigmann, Measurements of room-temperature band-gap-resonant optical nonlinearities of GaAs/AlGaAs multiple quantum wells and bulk GaAs, Appl. Phys. Lett. **52**, 1201 (1988).
[20] B. K. Ridley, *Quantum Processes in Semiconductors*, 3rd ed. (Oxford University Press, Oxford, 1993).
[21] S. Y. Mensah, F. K. A. Allotey, N. G. Mensah, and V. W. Elloh, Amplification of acoustic phonons in a degenerate semiconductor superlattice, Physica (Amsterdam) **19E**, 257 (2003).
[22] R. Loudon, The Raman effect in crystals, Adv. Phys. **13**, 423 (1964).
[23] J. C. Jackson, Thermal overstability in fusion plasmas—the SASER effect, Plasma Phys. Controlled Fusion **28**, 669 (1986).
[24] I. V. Volkov, S. T. Zavtrak, and I. S. Kuten, Theory of sound amplification by stimulated emission of radiation with consideration for coagulation, Phys. Rev. E **56**, 1097 (1997).